Inorganic Chemistry

Article

pubs.acs.org/IC

Field-Assisted Slow Magnetic Relaxation in a Six-Coordinate Co(II)−Co(III) Complex with Large Negative Anisotropy

Elena A. Buvaylo,[†] Vladimir N. Kokozay,[†] Olga Yu. Vassilyeva,*[,†] Brian W. Skelton,[‡] Andrew Ozarowski,[§] Ján Titiš,[#] Beáta Vranovičová,[#] and Roman Boča[#]

[†]Department of Chemistry, Taras Shevchenko National University of Kyiv, 64/13 Volodymyrska str., Kyiv 01601, Ukraine

[‡]School of Molecular Sciences, M310, University of Western Australia, Perth, WA 6009, Australia

[§]National High Magnetic Field Laboratory, Florida State University, 1800 E. Paul Dirac Drive, Tallahassee, FL 32310, United States

[#]Department of Chemistry, Faculty of Natural Sciences, University of SS Cyril and Methodius, 917 01 Trnava, Slovakia

Supporting Information

ABSTRACT: The reaction of $Co(CH_3COO)_2{\cdot}4H_2O$ with the Schiff base ligand LH_4 derived from *o*-vanillin and tris(hydroxymethyl)aminomethane produces the dinuclear mixed-valence complex $[Co^{II}Co^{III}(LH_2)_2(CH_3COO)(H_2O)](H_2O)_3$ (**1**), which has been investigated using IR spectroscopy, X-ray crystallography, temperature-dependent magnetic susceptibility, magnetization, HFEPR spectroscopy, and ac susceptibility measurements at various frequencies, temperatures, and external magnetic fields. The structure of **1** consists of neutral molecules in which two cobalt ions with distorted octahedral geometries, $Co^{II}O_6$ and $Co^{III}N_2O_4$, are bridged by two deprotonated $-CH_2O^-$ groups of the two LH_2^{2-} ligands. **1** completes a series with Cl, Br, NO_3, and NCS anions published before by different authors. Low-temperature HFEPR measurements reveal that the ground electronic state of the Co(II) center in **1** is a highly anisotropic Kramers doublet; the effective *g* values of 7.18, 2.97, and 1.96 are frequency-independent over the frequency ranges 200−630, 200−406, and 200−300 GHz for the highest, intermediate, and lowest g_{eff} values, respectively. The two lower values were not seen at higher frequencies because the magnetic field was not high enough. Temperature-dependent magnetic susceptibility and field-dependent magnetization data confirm high magnetic anisotropy of the easy axis type. Complex **1** behaves as a single-ion magnet under a small applied external field and demonstrates two relaxation modes that strongly depend on the applied static dc field. The observation of multiple relaxation pathways clearly distinguishes **1** from the Cl and Br analogues.

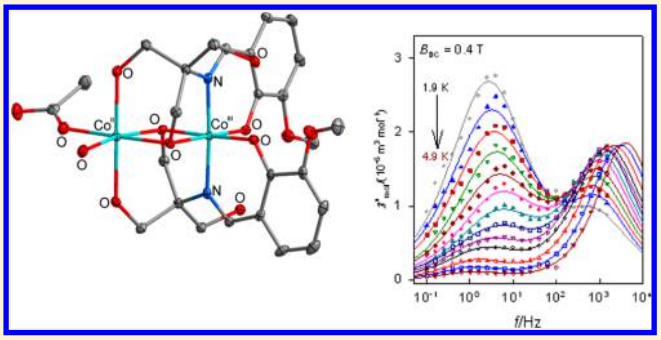

INTRODUCTION

Polynuclear molecular systems with a negative axial magnetic anisotropy on a high-spin ground state that show slow relaxation of magnetization at low temperature upon removal of a magnetizing field have been classified as single-molecule magnets (SMMs).[1] Their possible applications in high-density information storage, spintronics, and quantum computing make SMMs highly attractive to scientists, and research activity in the field is accelerating.[2] However, SMM behavior is not completely understood, and the synthesis of molecules with magnetic memory above room temperature remains elusive.

The slow relaxation of SMMs arises from their strong magnetic anisotropy, described mainly by the axial zero-field splitting (ZFS) parameter *D*, that results in an energy barrier for reversal of the magnetization.[3] Recent observations of slow magnetic relaxation effects in molecules including one single magnetic ion, so-called single-ion magnets (SIMs), confirm the dominant role of magnetic anisotropy in SMM design.[4] SIMs attract much attention as these species can exhibit significantly greater anisotropies than their multinuclear counterparts and appear to be simpler model systems for studying and understanding magnetic relaxation dynamics. Moreover, better synthetic control over many aspects of the composition and structure can be exerted in the case of mononuclear complexes.

As a large anisotropic ion, cobalt(II) is a good candidate for SIMs among 3d transition metals.[5] Most recently, it has been shown that the slow relaxation of cobalt(II) ions with nonuniaxial anisotropy in a model molecular complex and other similar systems is a general consequence of time-reversal symmetry that hinders direct spin−phonon processes regardless of the sign of the magnetic anisotropy.[6] Hexacoordinated high-spin Co(II) complexes usually display SMM behavior under a small applied external field that suppresses the fast magnetic tunneling.[7] There is still much to learn about mechanisms responsible for the slow magnetic relaxation in such systems, and increasing the anisotropy energy barrier is regarded as a highly desirable objective.

Received: March 7, 2017
Published: May 30, 2017

DOI: 10.1021/acs.inorgchem.7b00605
Inorg. Chem. 2017, 56, 6999−7009

Chart 1. Formation of LH_4 and Complex 1

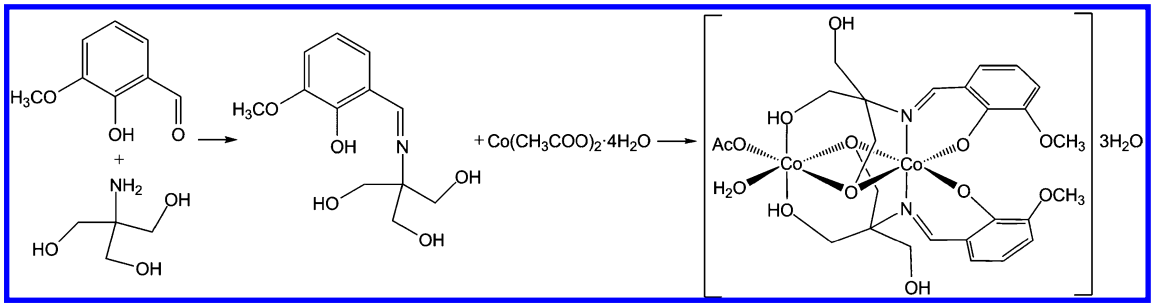

The title compound $[Co^{II}Co^{III}(LH_2)_2(CH_3COO)(H_2O)](H_2O)_3$ (**1**) [LH_4 = 2-{[(2-hydroxy-3-methoxyphenyl)-methylene]amino}-2-(hydroxymethyl)-1,3-propanediol, Chart 1] has been synthesized as part of our ongoing research on transition metal complexes of Schiff base ligands aimed at preparing new compounds of various nuclearity and structures with diverse potential advantages.[8] LH_4 was formed *in situ* from the condensation between *o*-vanillin and tris(hydroxymethyl)-aminomethane. Obviously, the Schiff base ligand should favor formation of polynuclear metal clusters due to the presence of the tripodal alcohol functionality. Indeed, crystal structures of about 30 metal complexes of LH_4 found in the Cambridge Database mostly comprise polynuclear Co_2, V_2, Cu_4, Mn_4, Ni_4, Ln_9, and Ln_{10} assemblies with a few examples of heterometallic 1s−3d and 3d−4f clusters of 4−20 nuclearity.[9] We also showed that LH_4 facilitated oxidation of Mn^{II} by stabilizing the Mn^{IV} oxidation state.[10a] The isolated $Mn^{IV}(LH_2)_2\cdot 0.39H_2O$ was subjected to thorough experimental and theoretical examination to understand the origin of ZFS in mononuclear octahedral Mn^{IV} complexes.[10b]

The structure of **1** is very similar to those previously reported in a series of $[Co^{II}Co^{III}(LH_2)_2(X)(H_2O)](H_2O)_m$ (X = Cl (**2**), Br (**3**), NO_3 (**4**); *m* = 3, 4)[5a] and $[Co^{II}Co^{III}(LH_2)_2(NCS)(CH_3OH)]\cdot 1.5CH_3OH\cdot 1.5H_2O$ (**5**)[11] complexes, where **2** and **3** show SIM behavior under an external dc field. The coordination geometry around the Co(II) ion in **2**−**5** is a distorted octahedron with pronounced elongation along the O−Co−O axis perpendicular to the $Co^{III}(O)_2Co^{II}$ fragment. It was found that the temperature dependences of the magnetic susceptibility of **2**−**5** are characteristic of noninteracting mononuclear Co(II) complexes with a considerable contribution from the orbital angular momentum; the compounds exhibit very similar $\chi_M T$ vs *T* plots with the $\chi_M T$ values in the ranges 2.89−3.18 and 1.77−2.0 $cm^3\ mol^{-1}\ K$ at 300 and 2 K, respectively. The use of the Griffith Hamiltonian for the description of the temperature dependences of the magnetic susceptibility of **2**−**4** along with analysis of the geometry of Co(II) polyhedron resulted in the conclusion about the positive sign of the axial field parameter Δ_{ax} and the ground state of the Co(II) ion being orbital singlet $^4A_{2g}$.[5a] At the same time, application of the ZFS spin-Hamiltonian to fit the field and temperature dependences of the magnetization of **2**−**4** led to negative *D* values of **2** and **3**, −7.4 and −9.7 cm^{-1}, respectively.

In the present paper, we report the synthesis, crystal structure, magnetic dc data, and a field-induced slow magnetic relaxation behavior of compound **1**, $[Co^{II}Co^{III}(LH_2)_2(CH_3COO)(H_2O)](H_2O)_3$, as well as quantum-chemical evaluation of the crystal field parameters and the results of the low-temperature, variable-frequency EPR study. The ground term of Co(II) magnetoactive ion in **1** is shown to be orbitally degenerate ^4E_g rather than $^4A_{2g}$, what makes application of the ZFS spin-Hamiltonian irrelevant. The dc magnetic data for **1** ($\chi_M T$ values of 3.06 and 1.91 $cm^3\ mol^{-1}\ K$ at 300 and 2 K, respectively) reveal a considerable magnetic anisotropy of an easy axis type; however, the traditional ZFS parameter $D < 0$ cannot be assigned.

EXPERIMENTAL SECTION

Reagents and General Procedures. 2-Hydroxy-3-methoxybenzaldehyde was purchased from Aldrich and used as received. All other chemicals were purchased from local suppliers and used without further purification. All solvents were of AP-grade. All the experiments were carried out in air. Elemental analyses for Co were performed with an ICP spectrometer (Fisons Instruments, ARL Model 3410+) and with a PerkinElmer 2400 analyzer for C, H, and N. The infrared (IR) spectrum was recorded on a PerkinElmer 1600 FT-IR spectrometer from a KBr pellet in the 400−4000 cm^{-1} region. In the syntheses, the condensation reaction was utilized without isolation of the resulting Schiff base.

Synthesis of $[Co^{II}Co^{III}(LH_2)_2(CH_3COO)(H_2O)](H_2O)_3$ (1). 2-Hydroxy-3-methoxybenzaldehyde (0.15 g, 1 mmol) and tris-(hydroxymethyl)aminomethane (0.12 g, 1 mmol) were added to methanol (20 cm^3) and the solution was stirred magnetically for 30 min. Next $Co(CH_3COO)_2\cdot 4H_2O$ (0.25 g, 1 mmol) was added to the yellow solution, and the mixture was heated to 323 K under stirring for 30 min. The resulting brown solution was filtered and allowed to stand at room temperature with slow evaporation. Brown prisms of the title compound were formed over several days. They were collected by filter-suction, washed with dry i-PrOH, and finally dried *in vacuo*. Yield: 60−70%. IR (KBr, cm^{-1}, Figure S1): 3632 (w), 3330 (s, b), 3166 (s, b), 2926 (s), 2870 (s), 2790 (w), 1632 (s), 1602 (s), 1564 (m), 1544 (m), 1472 (s), 1442 (s), 1406 (w), 1396 (m), 1318 (s), 1242 (s), 1220(s), 1170 (w), 1148 (w), 1104 (w), 1076 (m), 1014 (m), 978 (m), 862 (m), 742 (m), 600 (m), 560 (m), 490 (w), 434 (w). Anal. Calcd for $C_{26}H_{41}Co_2N_2O_{16}$ (755.47): C, 41.34; H, 5.47; N, 3.71; Co, 15.60%. Found: C, 40.99; H, 5.28; N, 4.02; Co, 15.34%.

Crystal Structure Determination. Crystallographic data for **1** were collected at 100(2) K on an Oxford Diffraction Xcalibur diffractometer using Mo Kα radiation. Following analytical absorption corrections and solution by direct methods, the structure was refined against F^2 with full-matrix least-squares using the program SHELXL-97.[12] Water molecule hydrogen atoms were located and refined with geometries restrained to ideal values. All other hydrogen atoms were added at calculated positions and refined by the use of a riding model with isotropic displacement parameters based on those of the parent atom. Anisotropic displacement parameters were employed for the non-hydrogen atoms. The crystal data and structure refinement are given in Table 1.

Magnetic Measurements. The magnetic measurements were conducted using a SQUID apparatus (MPMS-XL7, Quantum Design) in the RSO mode of detection. About 33 mg of the sample was encapsulated in a gelatin-made sample holder. The susceptibility taken at *B* = 0.5 T has been corrected for the underlying diamagnetism and converted to the effective magnetic moment. The magnetization has been measured at two temperatures: *T* = 2.0 and *T* = 4.6 K. The ac

DOI: 10.1021/acs.inorgchem.7b00605
Inorg. Chem. 2017, 56, 6999−7009

Table 1. Crystal Data and Structure Refinement for 1

formula	$C_{26}H_{41}Co_2N_2O_{16}$
formula weight	755.47
crystal system	monoclinic
space group	*Cc*
a/Å	12.6150(4)
b/Å	13.0039(10)
c/Å	19.0404(10)
β/deg	105.662(4)
V/Å^3	3007.5(3)
Z	4
ρ_c/g cm^{-3}	1.668
μ/mm^{-1}	1.184
crystal size/mm^3	0.19 × 0.09 × 0.07
θ range/deg	2.74−31.00
limiting indices	$-17 \le h \le 18$
	$-17 \le k \le 18$
	$-27 \le l \le 26$
no. of rflns collected	16 572
no. of independent rflns	7790 (R_{int} = 0.0392)
completeness to *θ*/%	99.0
absorption correction	analytical
max. and min transmission	0.965 and 0.920
refinement method	full-matrix least-squares on F^2
no. of data/restraints/params	7790/24/462
goodness-of-fit on F^2	1.030
final *R* indices ($I > 2\sigma(I)$)	*R*1 = 0.0389, *wR*2 = 0.0747
R indices (all data)	*R*1 = 0.0466, *wR*2 = 0.0776
absolute structure parameter	−0.008(9)
largest diff peak and hole/e Å^{-3}	0.676 and −0.535
CCDC no.	1440294

susceptibility measurements were done at B_{dc} = 0.1, 0.2, and 0.4 T using an oscillating field B_{ac} = 0.38 mT for 22 frequencies ranging between *f* = 0.1 and 1500 Hz. Ten scans were processed for each temperature−frequency point, and scattered data outside the interval of 1*σ* were omitted; the rest were averaged. About 8000 data points were processed.

HFEPR Spectroscopy. High-frequency and -field EPR (HFEPR) spectra were recorded using a home-built spectrometer at the EMR facility of NHMFL.[13] The instrument is a transmission-type device in which waves are propagated in cylindrical lightpipes. The microwaves were generated by a phase-locked oscillator (Virginia Diodes) operating at a frequency of 13 ± 1 GHz and generating its harmonics, of which the 4th, 8th, 16th, 24th, 32nd, and 48th were available. A superconducting magnet (Oxford Instruments) capable of reaching a field of 17 T was employed.

Quantum Chemical Calculations. *Ab initio* calculations were performed using the ORCA 3.0.3 computational package (see Supporting Information).[14] The zeroth-order regular approximation (ZORA) together with the scalar relativistic contracted version of TZVP basis functions has been applied. The calculations of ZFS parameters were based on state-averaged complete-active-space self-consistent field (SA-CASSCF) wave functions followed by *N*-electron valence second-order perturbation theory (NEVPT2). The active space of the CASSCF calculations consisted of seven electrons in five metal-based d-orbitals. The state averaged approach was used, in which all 10 quartet states and 40 doublets states were equally weighted. The calculations utilized the RI approximation with appropriate decontracted auxiliary basis set and the chain-of-spheres (RIJCOSX) approximation to exact exchange. Increased integration grids (Grid4) and tight SCF convergence criteria were used. The ZFS parameters were calculated through the quasi-degenerate perturbation theory in which an approximation to the Breit−Pauli form of the spin−orbit coupling operator (SOMF) and the effective Hamiltonian theory were utilized.

RESULTS AND DISCUSSION

Synthetic Aspects. Slow evaporation of methanol solution of stoichiometric (1:1) quantities of $Co(CH_3COO)_2{\cdot}4H_2O$ and the preformed Schiff base ligand resulted in the formation of brown crystals of **1** in a quantitative yield. Partial oxidation of the cobalt(II) atom to the cobalt(III) species proceeds easily in open air indicating that the tetradentate ligand LH_2^{2-} containing two O^- donors effectively stabilizes the $Co^{II}Co^{III}$ mixed-valence core.

Structure Description. Complex **1**, which crystallizes in the monoclinic space group *Cc*, is isomorphous with $[Co^{II}Co^{III}(LH_2)_2(NO_3)(H_2O)](H_2O)_3$[5a] and isostructural with the $[Co^{II}Co^{III}(LH_2)_2(X)(H_2O)](H_2O)_4$[5a] (X = Cl, Br) and $[Co^{II}Co^{III}(LH_2)_2(NCS)(CH_3OH)]{\cdot}1.5CH_3OH{\cdot}1.5H_2O$[11] analogues. The structure of **1** consists of isolated $[Co^{II}Co^{III}(LH_2)_2(CH_3COO)(H_2O)]$ neutral molecules in which two cobalt ions are bridged by two deprotonated $-CH_2O^-$ groups of the two LH_2^{2-} ligands; solvent water molecules are involved in a complex hydrogen-bonding network. The molecular diagram and numbering scheme of **1** is shown in Figure 1, selected bond and angle parameters are given in Table 2, and details of the hydrogen bonding are provided in the Supporting Information (Table S1).

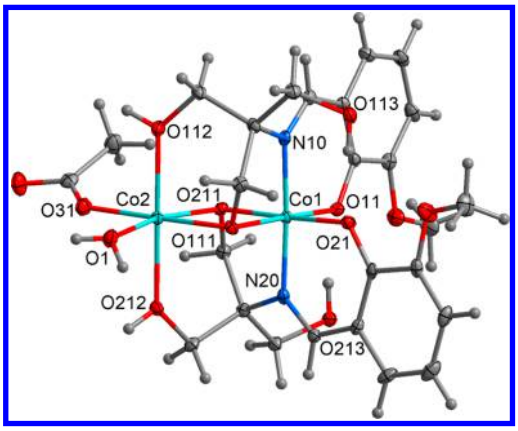

Figure 1. Molecular structure of **1** with principal labeling. Displacement ellipsoids for non-H atoms are drawn at the 50% probability level.

The $[Co^{II}Co^{III}(LH_2)_2(CH_3COO)(H_2O)]$ molecule shows no crystallographically imposed symmetry with two metal atoms in $Co(1)N_2O_4$ and $Co(2)O_6$ distorted octahedral geometries. The oxidation state assignments for the cobalt ions were made using charge considerations and interatomic distances. The Co−N/O bond lengths around Co(1) (1.89−1.90 Å) are shorter than the Co−O distances around Co(2) (2.03−2.16 Å), suggesting that Co(1) and Co(2) are Co(III) and Co(II), respectively. This is further supported by a tetragonal distortion of the geometry around Co(2), due to the Jahn−Teller effect of the Co(II) (d^7) ion (Table 2). The Co(2) bond lengths indicate the two shortest bonds being in *cis* configuration and two additional intermediate bonds being *cis* to the previous donors as well, which can be interpreted as an elongated tetragonal geometry (with the axis along O(112) and O(212)). The *cis* angles at the metal atoms lie in the ranges 86−96° (Co(1)) and 78−104° (Co(2)), and the *trans* ones vary from 176 to 177° (Co(1)) and from 164 to 179° (Co(2)). An extremely strong orthorhombic distortion stems from the

DOI: 10.1021/acs.inorgchem.7b00605
Inorg. Chem. 2017, 56, 6999−7009

Table 2. Bond Lengths/Å and Angles/deg in 1

Co(1)−N(10)	1.887(2)	Co(2)−O(31)	2.030(2)
Co(1)−N(20)	1.891(2)	Co(2)−O(211)	2.0357(19)
Co(1)−O(11)	1.8952(19)	Co(2)−O(111)	2.0754(19)
Co(1)−O(21)	1.8976(19)	Co(2)−O(1)	2.105(2)
Co(1)−O(211)	1.8981(19)	Co(2)−O(112)	2.139(2)
Co(1)−O(111)	1.8996(19)	Co(2)−O(212)	2.162(2)
N(10)−Co(1)−N(20)	176.90(10)	O(31)−Co(2)−O(211)	103.92(8)
N(10)−Co(1)−O(11)	96.14(9)	O(31)−Co(2)−O(111)	178.01(9)
N(20)−Co(1)−O(11)	86.04(9)	O(211)−Co(2)−O(111)	77.70(7)
N(10)−Co(1)−O(21)	85.81(9)	O(31)−Co(2)−O(1)	91.54(9)
N(20)−Co(1)−O(21)	96.33(9)	O(211)−Co(2)−O(1)	163.73(8)
O(11)−Co(1)−O(21)	92.13(9)	O(111)−Co(2)−O(1)	86.94(8)
N(10)−Co(1)−O(211)	91.65(9)	O(31)−Co(2)−O(112)	90.88(8)
N(20)−Co(1)−O(211)	86.09(9)	O(211)−Co(2)−O(112)	93.55(8)
O(11)−Co(1)−O(211)	91.16(8)	O(111)−Co(2)−O(112)	87.87(8)
O(21)−Co(1)−O(211)	176.05(9)	O(1)−Co(2)−O(112)	91.20(8)
N(10)−Co(1)−O(111)	86.30(9)	O(31)−Co(2)−O(212)	89.85(8)
N(20)−Co(1)−O(111)	91.40(9)	O(211)−Co(2)−O(212)	87.09(8)
O(11)−Co(1)−O(111)	175.96(9)	O(111)−Co(2)−O(212)	91.38(8)
O(21)−Co(1)−O(111)	91.26(8)	O(1)−Co(2)−O(212)	87.94(8)
O(211)−Co(1)−O(111)	85.55(8)	O(112)−Co(2)−O(212)	178.89(8)

rather acute value of O(211)−Co(2)−O(111) angle due to the bridging O atoms.

In the crystal structure, the paramagnetic Co(II) ions are magnetically well isolated from each other by the diamagnetic Co(III) ion, Schiff base ligands, coordinated acetate anion, and solvent water molecules. The shortest distance between the Co(II) ions of neighboring molecules is 9.059 Å.

Crystal Field Theory. The group theory offers for hexacoordinate high-spin Co(II) systems a branching diagram as shown in Chart 2. Note that in the D'_2 double group all multiplets span the doubly degenerate representation Γ_5 (Bethe notation).

Chart 2. Development of the Crystal Field Terms (T, A, E, B) and Spin−Orbit Multiplets (Γ_i) under Symmetry Lowering for Hexacoordinate Co(II) High-Spin Systems

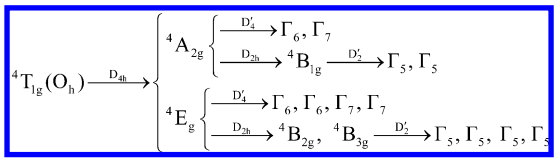

In order to bring more light into the energy levels of high-spin Co(II) systems with orthorhombic symmetry D_2 and D'_2, the generalized crystal field theory working in the complete space of 120 kets has been employed (see Supporting Information).[15] Using the Racah parameters B = 989, C = 4253 cm^{-1}, the spin−orbit coupling constant ξ = 515 cm^{-1}, and the crystal field poles for ligands situated in the *trans*-positions F_4 = 8500, 8000, and 5000 cm^{-1}, the calculated lowest crystal field terms arising from the mother $^4T_{1g}(O_h)$ term are $^4B_{2g}$ (ground), $^4B_{3g}$ (at 219 cm^{-1}), and $^4B_{1g}$ (at 1529 cm^{-1}). This result confirms that the ground electronic term is not well separated from the first excited term, and thus, the application of the perturbation theory in calculating the spin-Hamiltonian parameters suffers of divergence. When the spin−orbit interaction is included via the variation method, the calculated spin−orbit involving spectrum is 0, 213, 500, 761, 1917, and 1928 cm^{-1} (all Kramers doublets belong to Γ_5 representation of the D'_2 double group).

Of crucial importance is the fact that the two lowest Kramers doublets do not match the spin-Hamiltonian assumption: within the double group D'_4, both refer to the Γ_6 representation (Bethe notation) as opposed to the spin-Hamiltonian formalism that requires the Γ_6 (ground) and Γ_7 (excited) assignment (Table 3).

Table 3. Lowest Energy Levels

method	energy/cm^{-1}	
(a) Crystal Field Terms[a]	[^4E_g, $^4A_{2g}$], [$^4B_{2g}$, ^4E_g], $^4B_{1g}$, [$^4A_{2g}$, ^4E_g]	
quartet excitation energies (ORCA, NEVPT2)	[(0, 463), 1523], [7268, (8819, 9387)], 17666, [20102, (22623, 25579)]	
crystal field calculations	[(0, 219), 1529], [9329, (11794, 12218)], 23079, [24405, 24678, 24710]	
(b) Six Kramers Doublets (Spin−Orbit Multiplets)	From Ground ^4E_g ($^4B_{2g}$, $^4B_{3g}$) Term	From $^4A_{2g}$ ($^4B_{1g}$) Term
ORCA calculation	0, 219, 752, 1020	1867, 1942
crystal field calculation[b]	0 (Γ_6), 213 (Γ_6), 500 (Γ_7), 761 (Γ_7)	1917 (Γ_6), 1928 (Γ_7)
fit of dc magnetic data to Griffith−Figgis model	0, 179, 356, 593	1005, 1149

[a][]: daughter terms of octahedral T-terms on the reduction $O_h \rightarrow D_{4h}$: $T_{1g} \rightarrow E_g + A_{2g}$ or $T_{2g} \rightarrow E_g + B_{2g}$. (): daughter terms of E_g terms on the reduction $D_{4h} \rightarrow D_{2h}$: $E_g \rightarrow B_{2g} + B_{3g}$. [b]Irreducible representations within the D'_4 double group (Bethe notation).

Quantum-Chemical Calculations. *Ab initio* calculations were performed for the whole complex **1** containing 78 atoms in its experimental geometry as determined by the X-ray diffraction. The most informative is the calculated spectrum of energy levels that takes into account the spin−orbit coupling. The four lowest Kramers doublets at 0, 219, 752, and 1020 cm^{-1} are daughters of the orbitally degenerate $^4E(D_{4h})$ mother term and/or quasi-degenerate $\{^4B_{2g}, ^4B_{3g}\}(D_{2h})$ pair. Two remaining Kramers doublets at 1867 and 1942 cm^{-1} arise from the excited $^4A_{2g}$ ($^4B_{1g}$) term (Chart 2). This feature is a consequence of the geometry of the chromophore of **1** approximating an elongated tetragonal bipyramid. The crystal

DOI: 10.1021/acs.inorgchem.7b00605
Inorg. Chem. 2017, 56, 6999−7009

field splitting of the $^4T_{1g}(O_h)$ term is measured by the axial splitting parameter Δ_{ax} that with the ground $^4E_g(D_{4h})$ and excited $^4A_{2g}(D_{4h})$ terms adopts a negative value. This parameter induces a magnetic anisotropy corresponding to an easy axis of magnetization.

In the case of a degenerate ground electronic term ^4E_g, the spin-Hamiltonian formalism, conventionally accepted for the description of zero-field splitting of $S = 3/2$ cobalt ion in a distorted octahedral environment, is not legitimate to use. Indeed, activation of the spin-Hamiltonian formalism in the ORCA package brings values of $D/hc = -99.6$ cm^{-1}, $E/D = 0.27$, and g-factor components $g_1 = 1.824$, $g_2 = 2.317$, and $g_3 = 3.085$ ($g_{iso} = 2.409$). The value of $D < 0$ and $g_1 < 2.0$ are considered unphysical for Co(II) complexes with the geometry of an elongated tetragonal bipyramid.

HFEPR Measurements. The EPR spectra recorded over the frequency range 211−634 GHz are given in Figure 2.

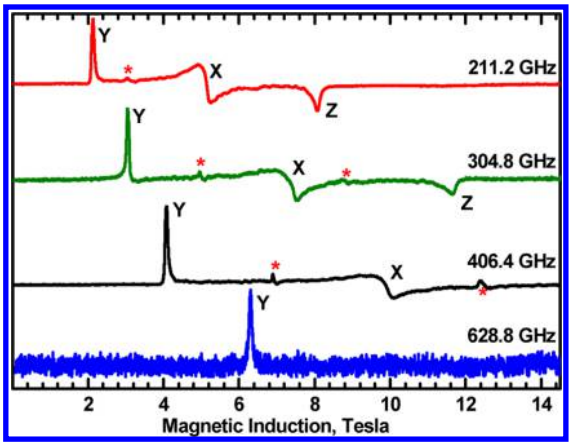

Figure 2. HFEPR spectra of **1** recorded at 5 K with various microwave frequencies. The "X", "Y", and "Z" features are observed at the effective g values of 2.97, 7.18, and 1.96, respectively. The effective g values are independent of the microwave frequency. Asterisks indicate resonances due to molecular oxygen ($S = 1$) adsorbed on the powder sample.

The spectra show a characteristic pattern of an $S = 3/2$ system with the zero-field splitting being much larger than the microwave quantum energy, and this is true even for the 628.8 GHz spectrum. Such cases are often interpreted in terms of an *effective* $S^* = 1/2$ state and *effective* g values. For complex **1**, we have three effective g components, 2.97, 7.18, and 1.96. The highest g_{eff} value was frequency independent over the frequency range 200−630 GHz. The two lower values were frequency independent when they were seen: the intermediate is over 200−406 GHz and the lowest is over 200−300 GHz. They were not seen at higher frequencies because the magnetic field was not high enough.

dc Magnetometry. The high-temperature limit of the effective magnetic moment for the $S = 3/2$ system is $\mu_{eff}(HT)/\mu_B = g[S(S+1)]^{1/2}$ which for $g_e = 2.0$ yields $\mu_{eff}(HT, g_e) = 3.87$ μ_B. The effective magnetic moment for **1** at the room temperature adopts a value of $\mu_{eff} = 4.97$ μ_B, and it slowly decreases until $T = 100$ K (Figure 3). These data show that the averaged magnetogyric factor is about $g_{av} = 2.57$. Below $T = 100$ K the decrease of the effective magnetic moment is more progressive, and at $T = 1.9$ K it is $\mu_{eff} = 3.92$ μ_B. This effect can be ascribed to a depopulation of the magnetic energy levels commonly termed zero-field splitting.

The magnetization per formula unit $M_1 = M_{mol}/(N_A\mu_B)$ at $B = 7$ T and $T = 2.0$ K adopts a saturation value of $M_1 = 2.57$ that is much lower than the spin-only value $M_1 = g_{av}S = 3.95$. This observation again confirms the presence of a sizable magnetic anisotropy.

For the ground term ^4E_g, arising from the $^4T_{1g}$ mother term, four Kramers doublets are thermally accessible, and evaluation of their energies requires involvement of the orbital angular momentum. There is no visible maximum at the μ_{eff} vs$T$ curve that matches features when the angular momentum is partially quenched by the crystal field of lower symmetry. Thus, on further symmetry lowering $D_{4h} \rightarrow D_{2h}$ the ground term $^4B_{2g}$ is no longer orbitally degenerate. However, application of the perturbation theory to obtain the spin-Hamiltonian parameters is problematic because of the existence of low-lying excited states.

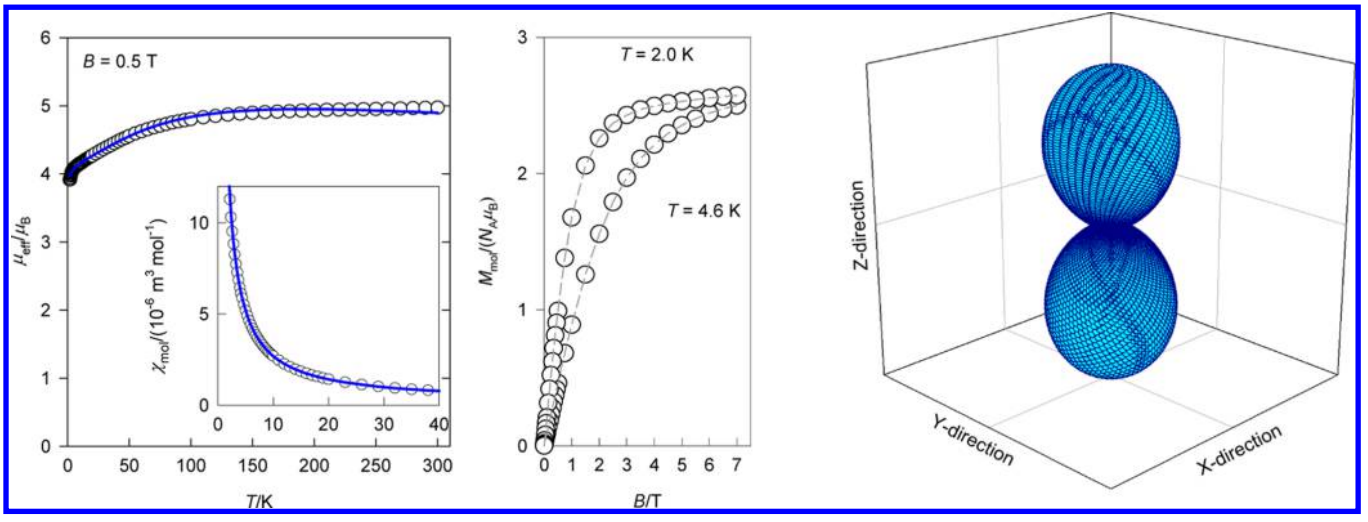

Figure 3. dc magnetic data for **1**. (Left) temperature dependence of the effective magnetic moment ((inset) temperature dependence of the molar magnetic susceptibility). (Center) field dependence of the magnetization per formula unit. Open symbols: experimental data. Solid lines: fitted with the extended Griffith−Figgis model. Dashed lines: a guide for eyes. (Right) 3D visualization of the magnetization reconstructed for $T = 2.0$ K and $B = 1.0$ T showing a negative magnetic anisotropy (easy axis of magnetization).

DOI: 10.1021/acs.inorgchem.7b00605
Inorg. Chem. 2017, 56, 6999−7009

Table 4. Structural and Magnetic Data for a Series of $[Co^{II}Co^{III}(LH_2)_2(X)(Solv)](Solv)_m$ Complexes[a]

	CH_3COO^-	Cl^-	Br^-	NO_3^-	NCS^-
abbr	**1**	**2**	**3**	**4**	**5**
ref	this work	5a	5a	5a	11
		Distances Co^{II}–L/Å			
$Co^{II}–X_{eq}$	2.031	2.396	2.554	1.997	2.042
$Co^{II}–O_{eq}$	2.075	2.067	2.072	2.086	2.044
$Co^{II}–O_{eq}$	2.036	2.049	2.054	2.035	2.037
$Co^{II}–O_{eq}$	2.105(w)	2.083(w)	2.068(w)	2.129(w)	2.097(OMe)
$av(Co^{II}–O)_{eq}$	2.062	2.066	2.065	2.062	2.055
$Co^{II}–O_{ax}$	2.139	2.132	2.155	2.142	2.143
$Co^{II}–O_{ax}$	2.162	2.184	2.154	2.164	2.170
$av(Co^{II}–O)_{ax}$	2.150	2.158	2.154	2.153	2.156
		Magnetic Parameters[b]			
g	2.36, 2.87	2.32	2.52		2.33
D/cm^{-1}	(145)	−7.4	−9.7		|18.7|
E/cm^{-1}					0.12

[a]w = aqua ligand. [b]Magnetic parameters obtained within ZFS spin-Hamiltonian formalism.

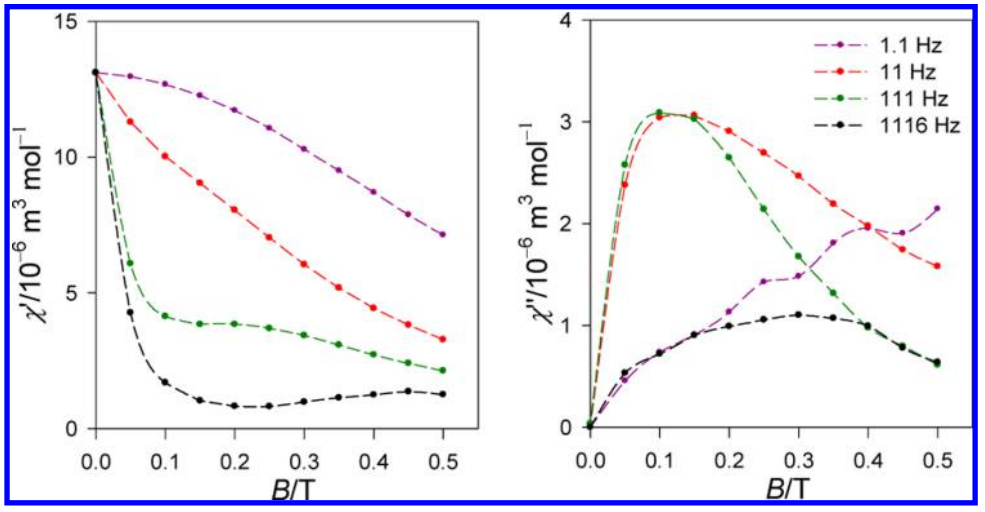

Figure 4. In-phase χ' (left) and out-of-phase χ'' molar susceptibility (SI units) for **1** with dependence upon external magnetic field B_{dc} at T = 2.0 K. The lines are drawn to guide the eye.

The Hamiltonian appropriate for such a system was proposed by Griffith[16] and further modified by Figgis:[17]

$$\hat{H}^{GF} = -A\kappa\lambda(\vec{L}_p\cdot\vec{S})\hbar^{-2} + \mu_B\vec{B}\cdot(g_e\vec{S} - A\kappa\vec{L}_p)\hbar^{-1} + [\Delta_{ax}(\hat{L}_{p,z}{}^2 - \vec{L}_p{}^2/3) + \Delta_{rh}(\hat{L}_{p,x}{}^2 - \hat{L}_{p,y}{}^2)]\hbar^{-2} \quad (1)$$

It accounts for the spin Zeeman term, orbital Zeeman term (within the T–p isomorphism), spin–orbit coupling, and the axial distortion term and involves the spin–orbit splitting parameter $\lambda = -\xi/2S$, the orbital reduction factor κ, the Figgis CI parameter A, and the axial and rhombic splitting parameters Δ_{ax} and Δ_{rh}, respectively. Owing to the T–p isomorphism, the orbital angular momentum refers to $L_p = 1$. This Hamiltonian was treated in a fully numerical way resembling the common Hamiltonian for a dinuclear exchange interaction with axial and rhombic zero-field splitting. The susceptibility data were fitted with a reasonable set of magnetic parameters: $(A\kappa\lambda)/hc = -176$ cm^{-1}, $g_L = -(A\kappa) = -1.49$, $\Delta_{ax}/hc = -711$ cm^{-1}, $\Delta_{rh}/hc = 44$ cm^{-1}, molecular-field correction $zj/hc = -0.016$ cm^{-1}, and temperature-independent term $\chi_{TIM} = -6.5 \times 10^{-9}$ m^3 mol^{-1} [discrepancy factors $R(\chi) = 0.017$, $R(M) = 0.19$]. This set, however, underestimates the magnetization data. The reconstructed magnetic energy levels are listed in Table 3 and compared with theoretical calculations.

Structural and magnetic data for a set of similar dinuclear complexes $[Co^{II}Co^{III}(LH_2)_2(X)(Solv)](Solv)_m$, differing in the anionic ligand X^-, are summarized in Table 4. Similarly to **1**, the donor atom of the ligand X^- in **2**–**5** can be set to an equatorial position along with three O donors originated from the ligands and water/methanol molecules. The average Co^{II}–O/N distances in the equatorial plane then will be roughly the same for all five compounds: $(Co^{II}–O/N)_{eq}$ = 2.06 Å; the axial ones amount to $av(Co^{II}–O)_{ax}$ = 2.15. Thus, the Co(II) coordination polyhedron in the case of **2**–**5** can also be viewed as an elongated square bipyramid for which the spin-Hamiltonian formalism is not applicable. However, some data along these lines have been reported for **2**–**5**,[5a,11] although for hexacoordinate Co(II) complexes much higher D values are typical.[18−20] The use of the ZFS spin-Hamiltonian in the form appropriate to the mononuclear Co(II), S = 3/2 to fit the magnetic dc data of **1** resulted in the positive D value of 145 cm^{-1} in contrary to the negative Δ_{ax} (see Supporting Information).

DOI: 10.1021/acs.inorgchem.7b00605
Inorg. Chem. 2017, 56, 6999−7009

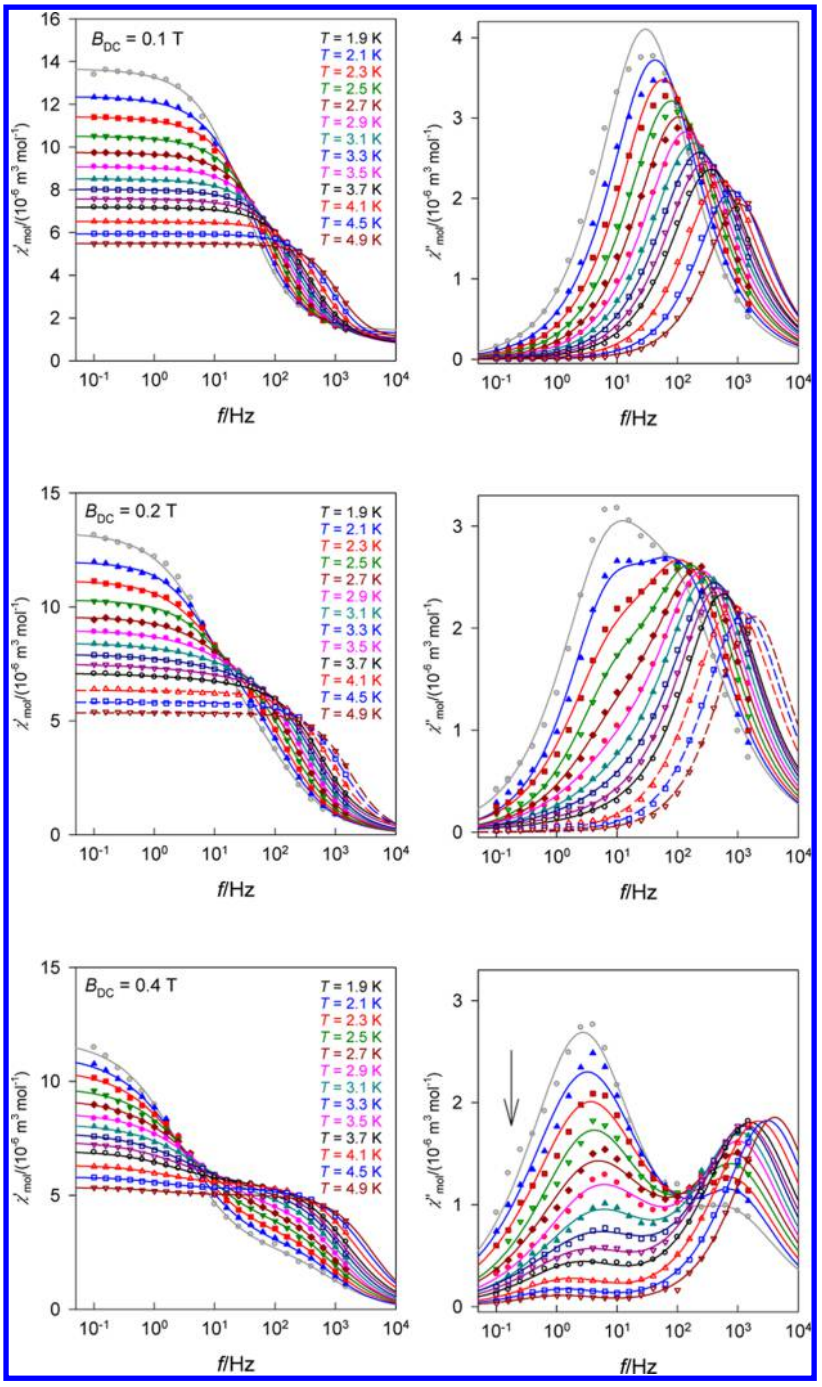

Figure 5. Frequency dependence of the ac susceptibility components for a fixed temperature at different applied dc fields: (left) in-phase component; (right) out-of-phase component (temperature evolution is the same as shown for the in-phase component). Solid lines: fitted with the single-component and/or two-component Debye model.

This finding supports the conclusion made by the authors of ref 7b that, in contrast to the Griffith and pseudo-spin-1/2 Hamiltonians, the applicability of the ZFS spin-Hamiltonian is often controversial. It was stressed that the Griffith Hamiltonian (or the corresponding pseudo-spin-1/2 Hamiltonian) represents the most suitable tool for the treatment of the magnetic data. This approach was successfully applied to analyze the magnetic data of the two-dimensional coordination polymer $[Co(dca)_2(atz)_2]_n$ resulting from assembling *trans*-bis(2-amino-1,3,5-triazine)cobalt(II) motifs by dicyanamide spacers.[7g] Its magnetically isolated high-spin cobalt(II) ions with a CoN_6 coordination environment of an elongated octahedron were shown to act as single-ion magnets under an applied magnetic field.

ac Magnetic Data. Complex **1** has been probed for slow magnetic relaxation using the ac susceptibility measurements. First, the effect of the applied dc field was monitored as shown in Figure 4. At zero magnetic field, the out-of-phase susceptibility is zero, which confirms a fast magnetic relaxation. However, with increasing dc field, the ac susceptibility signal becomes positive and it develops in a complex manner depending on the frequency of the applied oscillating field. This stimulated detailed data taking for a number of

DOI: 10.1021/acs.inorgchem.7b00605
Inorg. Chem. 2017, 56, 6999−7009

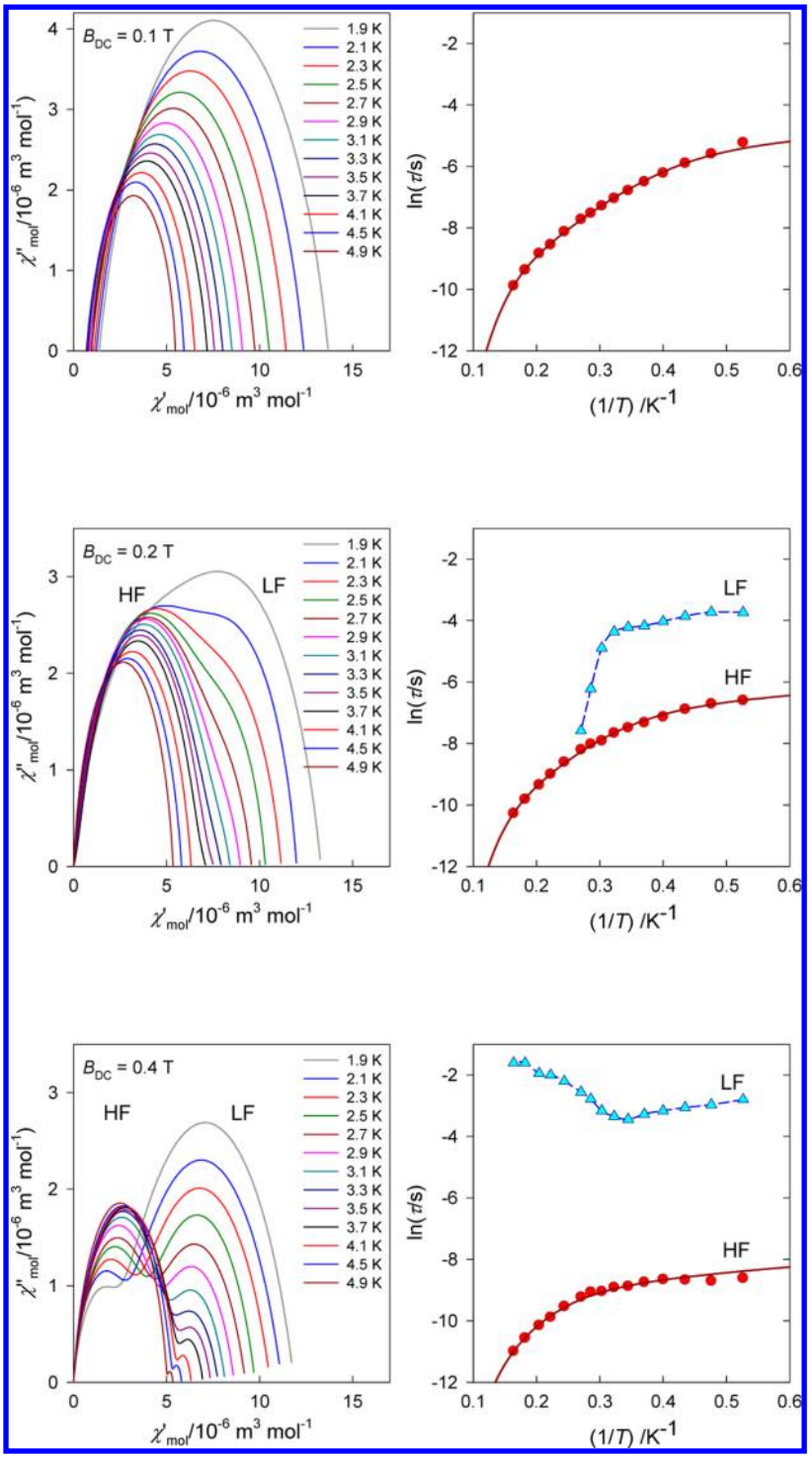

Figure 6. Fitted ac susceptibility data for **1** at B_{dc} = 0.1, 0.2, and 0.4 T: (left) Argand diagram; (right) Arrhenius-like plot with solid curves fitted according to eq 2.

frequencies, temperatures, and applied dc fields (B_{dc} = 0.1, 0.2, and 0.4 T).

A representative frequency dependence of the ac susceptibility components for a set of fixed temperatures is presented in Figure 5. At B_{dc} = 0.2 T two maxima exist. The low-frequency (LF) branch lies at about f = 10 Hz, and it progressively escapes with temperature; above T = 3 K it is hardly visible as a small tail. The high-frequency (HF) branch moves its maximum from $f = 10^2$ to $f > 10^3$ Hz. Such a shift allows us to conclude that **1** is a single-molecule (single-ion) magnet.

Both the in-phase and out-of-phase susceptibility components were fitted simultaneously to an extended, two-component Debye model (see Supporting Information) by minimizing the error functional defined as $F = R_1(\chi') \times R_2(\chi'')$ where R_1 and R_2 = relative errors.[21] The optimum parameters were used in reconstructing the interpolation/extrapolation lines drawn in Figure 5. The individual parameters along with their standard deviations are listed in the Supporting Information. As the LF branch progressively disappears on

DOI: 10.1021/acs.inorgchem.7b00605
Inorg. Chem. 2017, 56, 6999−7009

Table 5. SMM Parameters from the ac Susceptibility for 1 Referring to the High-Frequency (Faster) Branch

complex	B_{dc}/T	(U/k_B)/K	τ_0/s	m	$A/T^{-m}\ K^{-1}\ s^{-1}$	n	$C/K^{-n}\ s^{-1}$	ref
1	0.1	16.1(7)	$7.1(9) \times 10^{-6}$	4	$1.0(2) \times 10^{6}$	9	$0.76(3) \times 10^{-3}$	this work
1	0.2	18.0(10)	$3.2(7) \times 10^{-6}$	4	$2.3(2) \times 10^{5}$	9	$0.87(8) \times 10^{-3}$	this work
1	0.4	24.4(39)	$0.59(49) \times 10^{-6}$	4	$1.43(9) \times 10^{4}$	9	$1.2(6) \times 10^{-3}$	this work
2, Cl-analogue	0.1	7.9	6.1×10^{-6}					5a
3, Br-analogue	0.1	14.5	1.0×10^{-6}					5a
$[Co(abpt)_2(tcm)_2]$[a]	0.3	86	1.4×10^{-9}	2	2.879×10^{3}	4	7.30	23

[a]abpt = 4-amino-3,5-bis(2-pyridyl)-1,2,4-triazole; tcm = tricyanomethanide.

heating, above T = 4 K only a single-component Debye function has been utilized for data fitting (dashed lines).

The biplot of the ac susceptibility components is presented in Figure 6. It can be seen that such an Argand diagram is represented by two overlapped and distorted arcs. The relaxation times τ_1 and τ_2 refer to the frequency at which the χ'' displays the maximum; they enter the Arrhenius-like plot as shown in Figure 6, right. It is seen that the HF branch behaves in a standard way; i.e., at low temperatures it approaches a constant in the limit (tunneling process) whereas at higher temperatures its slope stays constant (Orbach process). The LF branch follows the expected dependence at low temperatures, but at higher temperatures it progressively disappears. The faster relaxation branch (HF) was processed by eq 2 that reflects the Orbach, direct, and Raman relaxation processes:

$$\tau^{-1} = \tau_0^{-1}\exp(-U/k_BT) + AB^mT + CT^n \quad (2)$$

Here m = 4 and n = 9 have been selected in accordance with recommendations for a Kramers ion with an insulated ground doublet.[22] The fitting procedure gave the parameters listed in Table 5. The barrier to spin reversal, U, falls in the expected range, and the extrapolated relaxation time τ_0 is also typical for SMM of this class.[7a] It must be mentioned, however, that the parameters fitted to the curved Arrhenius-like plot could differ from a primitive approach when some high-temperature data are processed via the linear equation $\ln \tau = \ln \tau_0 + (U/k_B)/T$.

Lowering the external field to B_{dc} = 0.1 T manifests itself in visible changes in the χ'' vs f function: the two peaks for LF and HF branches merge to a single peak, which is, however, asymmetric. The fitting procedure with a single Debye component is appropriate for T > 2.7 K. For lower temperatures, the single-component Debye function declines from the recorded envelope of two, close lying primitive functions. Unlike the B_{dc} = 0.2 T case, some residual adiabatic susceptibility χ_S remains.

Strengthening of the external field to B_{dc} = 0.4 T causes the LF peak to dominate at low temperatures. On heating, its height decreases in favor of the HF peak. Again a double-component Debye function has been applied in fitting the ac susceptibility data. The fitting procedure is less successful due to the onset of the third branch (marked by an arrow in Figure 5) at even lower frequencies (eLF) about f = 0.1−1.0 Hz.

Existence of the several relaxation channels has been documented recently for a number of Co(II) complexes, such as the tetracoordinate systems $[Co(biq)Cl_2]$, $[Co(biq)Br_2]$, $[Co(biq)I_2]$,[24] $[Co(Me_6tren)Cl]ClO_4$,[25] and $[Co(PPh_3)_2Br_2]$[26] and the pentacoordinate system $[CoL^3Cl_2]$[27] (biq = 2,2′-biquinoline; Me_6tren = tris[2-(dimethylamino)ethyl]amine; L^3 = 4-hept-1-ynyl-2,6-dipyrazol-1-ylpyridine). Also, the first hexacoordinate Ni(II) complex and Cu(II) analogue reported as SMMs possess two relaxation modes.[28] The same holds true for a mononuclear Mn(II) complex where the D value is negligible.[29] Some Dy(III) systems show two or three relaxation branches as well, e.g., the $\{Dy^{III}Cu^{II}\}_2$ complex.[30] In all cases, the LF channel is better developed on raising the applied dc field, and it disappears progressively on heating. Intermolecular contacts, such as $\pi-\pi$ stacking at short C···C distance, could be *raisons d'etre* of the LF branch. However, in some systems, such as $[Co(PPh_3)_2Br_2]$,[26] $[Co(Me_6tren)Cl]ClO_4$,[25] and **1**, the nature of the LF mode so far remains unknown. Unusual thermal development of the $\ln \tau$ vs T^{-1} for the LF branch (slight decrease and then visible increase with temperature) has already been reported for several Co(II) and Mn(II) complexes.[29]

CONCLUSIONS

The complex under study, $[Co^{II}Co^{III}(LH_2)_2(X)(H_2O)](H_2O)_3$ with X = CH_3COO^- (**1**), completes a series with X = Cl^- (**2**), Br^- (**3**), NO_3^-, and NCS^- analogues. The coordination polyhedron resembles an elongated tetragonal bipyramid for which the axial crystal field splitting parameter is negative: $\Delta_{ax}/hc \approx -700\ cm^{-1}$. In such a case the electronic ground term is orbitally degenerate $^4E_g(D_{4h})$. The spin−orbit interaction causes its splitting into a set of four Kramers doublets assigned as Γ_6 (ground), Γ_6, Γ_7, and Γ_7 that do not match the spin-Hamiltonian formalism. Magnetic data (magnetic susceptibility and magnetization) for **1** reveal a considerable magnetic anisotropy of an easy axis type, though the traditional zero-field splitting parameter D < 0 cannot be assigned from the formalism reasoning.

The ac susceptibility data show that **1** exhibits field-induced single-ion magnetism. At B_{dc} = 0.1 T a single peak at the χ'' vs f dependence is evident similarly to complexes **2** and **3**. Also, the SMM parameters such as the barrier to spin reversal and the extrapolated relaxation time for **1**−**3** are similar. On raising the magnetic field to B_{dc} = 0.2 and 0.4 T, respectively, two peaks appear: they refer to low-frequency (LF) relaxation and high-frequency (HF) relaxation branches, respectively. The HF branch behaves analogously to B_{dc} = 0.1 T and also to **2** and **3** at this field. A new LF branch is visible only at low temperatures, and on heating it tends to disappear.

Compound **1** together with its chemical analogues from the $\{Co^{II}Co^{III}\}$ family are a good example to demonstrate that interpretation of the magnetic behavior of the high-spin Co(II)-based SIMs with uniaxial anisotropy is not straightforward. In the case of a negative axial field, the application of a ZFS spin-Hamiltonian to describe magnetic characteristics of the system may result in noncorrespondence of the signs of Δ_{ax} and D parameters or lead to ambiguous D values. Compound **1** also shows that it is not always possible to obtain a direct access to the sign of the magnetic anisotropy by the use of low-temperature HFEPR techniques.

DOI: 10.1021/acs.inorgchem.7b00605
Inorg. Chem. 2017, 56, 6999−7009

■ ASSOCIATED CONTENT

Supporting Information

The Supporting Information is available free of charge on the ACS Publications website at DOI: 10.1021/acs.inorgchem.7b00605.

Details of hydrogen bonding, IR spectrum, the ORCA input file, details of the crystal field and Griffith−Figgis model calculations, additional ac susceptibility data, and complete set of the fitted magnetic data (PDF)

Accession Codes

CCDC 1440294 contains the supplementary crystallographic data for this paper. These data can be obtained free of charge via www.ccdc.cam.ac.uk/data_request/cif, by emailing data_request@ccdc.cam.ac.uk, or by contacting The Cambridge Crystallographic Data Centre, 12, Union Road, Cambridge CB2 1EZ, UK; fax: +44 1223 336033.

■ AUTHOR INFORMATION

Corresponding Author

*E-mail: vassilyeva@univ.kiev.ua. (O.Yu. Vassilyeva)

ORCID

Olga Yu. Vassilyeva: 0000-0002-4315-8399

Andrew Ozarowski: 0000-0001-6225-9796

Roman Boča: 0000-0003-0222-9434

Notes

The authors declare no competing financial interest.

■ ACKNOWLEDGMENTS

Grant Agencies (Slovakia: APVV-0078-14 and VEGA 1/0534/16) are acknowledged for the financial support. The HFEPR spectra were recorded at the NHMFL which is supported by the NSF through the cooperative agreement DMR-1157490, the State of Florida and the Department of Energy. The authors acknowledge access to the facilities at the Centre for Microscopy, Characterisation and Analysis, University of Western Australia. Research support by the COST Action CM1305 ECOSTBio (Explicit Control Over Spin-States in Technology and Biochemistry) is gratefully acknowledged.

■ REFERENCES

(1) Gatteschi, D.; Sessoli, R.; Villain, J. *Molecular Nanomagnets*; Oxford University Press, Inc.: New York, 2006.

(2) (a) Wernsdorfer, W.; Sessoli, R. Quantum phase interference and parity effects in magnetic molecular clusters. *Science* **1999**, *284*, 133. (b) Leuenberger, N. M.; Loss, D. Quantum computing in molecular magnets. *Nature* **2001**, *410*, 789. (c) Meier, F.; Loss, D. Coherent spin quantum dynamics in antiferromagnetic rings. *Phys. B* **2003**, *329*, 1140. (d) Bogani, L.; Wernsdorfer, W. Molecular spintronics using single-molecule magnets. *Nat. Mater.* **2008**, *7*, 179.

(3) (a) Villain, J.; Hartman-Boutron, F.; Sessoli, R.; Rettori, A. Magnetic Relaxation in Big Magnetic Molecules. *Europhys. Lett.* **1994**, *27*, 159. (b) Luis, F.; Bartolomé, J.; Fernández, J. F. Resonant magnetic quantum tunneling through thermally activated states. *Phys. Rev. B* **1998**, *57*, 505.

(4) (a) Rinehart, J. D.; Long, J. R. Slow magnetic relaxation in a trigonal prismatic uranium(III) complex. *J. Am. Chem. Soc.* **2009**, *131*, 12558. (b) Freedman, D. E.; Harman, W. H.; Harris, T. D.; Long, G. J.; Chang, C. J.; Long, J. R. Slow magnetic relaxation in a high-spin iron(II) complex. *J. Am. Chem. Soc.* **2010**, *132*, 1224. (c) Baldoví, J. J.; Cardona-Serra, S.; Clemente-Juan, J. M.; Coronado, E.; Gaita-Ariño, A.; Palii, A. Rational design of single-ion magnets and spin qubits based on mononuclear lanthanoid complexes. *Inorg. Chem.* **2012**, *51*, 12565.

(5) (a) Chandrasekhar, V.; Dey, A.; Mota, A. J.; Colacio, E. Slow Magnetic Relaxation in Co(III)−Co(II) Mixed-Valence Dinuclear Complexes with a $Co^{II}O_5X$ (X = Cl, Br, NO_3) Distorted-Octahedral Coordination Sphere. *Inorg. Chem.* **2013**, *52*, 4554. (b) Zhu, Y. Y.; Cui, C.; Zhang, Y. Q.; Jia, J. H.; Guo, X.; Gao, C.; Qian, K.; Jiang, S. D.; Wang, B. W.; Wang, Z. M.; Gao, S. Zero-field slow magnetic relaxation from single Co(II) ion: a transition metal single-molecule magnet with high anisotropy barrier. *Chem. Sci.* **2013**, *4*, 1802. (c) Zadrozny, J. M.; Long, J. R. Slow magnetic relaxation at zero field in the tetrahedral complex $[Co(SPh)_4]^{2-}$. *J. Am. Chem. Soc.* **2011**, *133*, 20732. (d) Fataftah, M. S.; Zadrozny, J. M.; Rogers, D. M.; Freedman, D. E. A mononuclear transition metal single-molecule magnet in a nuclear spin-free ligand environment. *Inorg. Chem.* **2014**, *53*, 10716.

(6) Gómez-Coca, S.; Urtizberea, A.; Cremades, E.; Alonso, P. J.; Camón, A.; Ruiz, E.; Luis, F. Origin of slow magnetic relaxation in Kramers ions with non-uniaxial anisotropy. *Nat. Commun.* **2014**, *5*, 4300.

(7) (a) Craig, G. A.; Murrie, M. 3d single ion magnets. *Chem. Soc. Rev.* **2015**, *44*, 2135 and refs therein. (b) Palii, A. V.; Korchagin, D. V.; Yureva, E. A.; Akimov, A. V.; Misochko, E. Y.; Shilov, G. V.; Talantsev, A. D.; Morgunov, R. B.; Aldoshin, S. M.; Tsukerblat, B. S. Single-Ion Magnet $Et_4N[Co^{II}(hfac)_3]$ with Nonuniaxial Anisotropy: Synthesis, Experimental Characterization, and Theoretical Modeling. *Inorg. Chem.* **2016**, *55*, 9696. (c) Plenk, C.; Krause, J.; Rentschler, E. A click-functionalized single molecule magnet based on cobalt(II) and its analogous manganese(II) and zinc(II) compounds. *Eur. J. Inorg. Chem.* **2015**, *2015*, 370. (d) Ishikawa, R.; Horii, Y.; Nakanishi, R.; Ueno, S.; Breedlove, B. K.; Yamashita, M.; Kawata, S. Field-induced single-ion magnetism based on single-phonon relaxation in a distorted octahedral high-spin cobalt(II) complex. *Eur. J. Inorg. Chem.* **2016**, *2016*, 3233. (e) Zhu, Y. Y.; Zhu, M. S.; Yin, T. T.; Meng, Y. S.; Wu, Z. Q.; Zhang, Y. Q.; Gao, S. Cobalt(II) coordination polymer exhibiting single-ion-magnet-type field-induced slow relaxation behavior. *Inorg. Chem.* **2015**, *54*, 3716. (f) Liu, X.; Sun, L.; Zhou, H.; Cen, P.; Jin, X.; Xie, G.; Chen, S.; Hu, Q. Single-ion-magnet behavior in a two-dimensional coordination polymer constructed from Co^{II} nodes and a pyridylhydrazone derivative. *Inorg. Chem.* **2015**, *54*, 8884. (g) Palion-Gazda, J.; Klemens, T.; Machura, B.; Vallejo, J.; Lloret, F.; Julve, M. Single ion magnet behaviour in a two-dimensional network of dicyanamide-bridged cobalt(II) ions. *Dalton Trans.* **2015**, *44*, 2989.

(8) (a) Nesterov, D. S.; Nesterova, O. V.; Kokozay, V. N.; Pombeiro, A. J. L. Polynuclear Heterometallic Complexes from Metal Powders: The "Direct Synthesis" Approach. *Eur. J. Inorg. Chem.* **2014**, *2014*, 4496. (b) Chygorin, E. N.; Kokozay, V. N.; Omelchenko, I. V.; Shishkin, O. V.; Titiš, J.; Boča, R.; Nesterov, D. S. Direct synthesis of a $\{Co^{III}_6Fe^{III}_6\}$ dodecanuclear complex, revealing an unprecedented molecular structure type. *Dalton Trans.* **2015**, *44*, 10918. (c) Nesterova, O. V.; Chygorin, E. N.; Kokozay, V. N.; Omelchenko, I. V.; Shishkin, O. V.; Boča, R.; Pombeiro, A. J. L. A self-assembled octanuclear complex bearing the uncommon close-packed $\{Fe_4Mn_4(\mu_4\text{-}O)_4(\mu\text{-}O)_4\}$ molecular core. *Dalton Trans.* **2015**, *44*, 14918.

(9) Groom, C. R.; Allen, F. H. The Cambridge Structural Database in Retrospect and Prospect. *Angew. Chem., Int. Ed.* **2014**, *53*, 662.

(10) (a) Buvaylo, E. A.; Vassilyeva, O. Y.; Skelton, B. W. *Acta Crystallogr.* **2015**, *E71*, 1307. (b) Zlatar, M.; Gruden, M.; Vassilyeva, O. Y.; Buvaylo, E. A.; Ponomarev, A. N.; Zvyagin, S. A.; Wosnitza, J.; Krzystek, J.; Garcia-Fernandez, P.; Duboc, C. Origin of the Zero-Field Splitting in Mononuclear Octahedral Mn^{IV} Complexes: A Combined Experimental and Theoretical Investigation. *Inorg. Chem.* **2016**, *55*, 1192.

(11) Zhu, W.; Zhang, S.; Cui, C.; Bi, F.; Ke, H.; Xie, G.; Chen, S. New dinuclear cobalt (II, III) and tetranuclear manganese (III) complexes assembled by a polydentate Schiff-base ligand: synthesis, structure and magnetic properties. *Inorg. Chem. Commun.* **2014**, *46*, 315.

(12) Sheldrick, G. M. *Acta Crystallogr., Sect. A: Found. Crystallogr.* **2008**, *64*, 112.

(13) Hassan, A. K.; Pardi, L. A.; Krzystek, J.; Sienkiewicz, A.; Goy, P.; Rohrer, M.; Brunel, L.-C. Ultrawide Band Multifrequency High-Field

DOI: 10.1021/acs.inorgchem.7b00605
Inorg. Chem. 2017, 56, 6999−7009

EMR Technique: A Methodology for Increasing Spectroscopic Information. *J. Magn. Reson.* **2000**, *142*, 300.
(14) (a) Neese, F. The ORCA program system, Wiley Interdiscip. *Rev. Comput. Mol. Sci.* **2012**, *2*, 73. (b) Neese, F. ORCA – An *Ab Initio*, Density Functional and Semi-empirical Program Package, Version 3.0.3. (c) Atanasov, M.; Ganyushin, D.; Pantazis, D. A.; Sivalingam, K.; Neese, F. Detailed Ab Initio First-Principles Study of the Magnetic Anisotropy in a Family of Trigonal Pyramidal Iron(II) Pyrrolide Complexes. *Inorg. Chem.* **2011**, *50*, 7460. (d) Angeli, C.; Borini, S.; Cestari, M.; Cimiraglia, R. A quasidegenerate formulation of the second order n-electron valence state perturbation theory approach. *J. Chem. Phys.* **2004**, *121*, 4043. (e) Angeli, C.; Cimiraglia, R.; Evangelisti, S.; Leininger, T.; Malrieu, J.-P. Introduction of n-electron valence states for multireference perturbation theory. *J. Chem. Phys.* **2001**, *114*, 10252. (f) Angeli, C.; Cimiraglia, R.; Malrieu, J.-P. n-electron valence state perturbation theory: A spinless formulation and an efficient implementation of the strongly contracted and of the partially contracted variants. *J. Chem. Phys.* **2002**, *117*, 9138. (g) Neese, F. Efficient and accurate approximations to the molecular spin-orbit coupling operator and their use in molecular g-tensor calculations. *J. Chem. Phys.* **2005**, *122*, 034107. (h) Ganyushin, D.; Neese, F. First-principles calculations of zero-field splitting parameters. *J. Chem. Phys.* **2006**, *125*, 024103. (i) Neese, F. Calculation of the zero-field splitting tensor on the basis of hybrid density functional and Hartree-Fock theory. *J. Chem. Phys.* **2007**, *127*, 164112.
(15) Boča, R. Magnetic Parameters and Magnetic Functions in Mononuclear Complexes Beyond the Spin-Hamiltonian Formalism. *Struct. Bonding (Berlin)* **2006**, *117*, 1.
(16) Griffith, J. S. *The Theory of Transition Metal Ions*; University Press: Cambridge, U.K., 1964.
(17) (a) Figgis, B. N. *Introduction to Ligand Fields*; Wiley: New York, 1966. (b) Figgis, B. N.; Gerloch, M.; Lewis, J.; Mabbs, F. E.; Webb, G. A. The magnetic behaviour of cubic-field $^4T_{1g}$ terms in lower symmetry. *J. Chem. Soc. A* **1968**, 2086.
(18) (a) Lohr, L. L.; Miller, J. C.; Sharp, R. R. Electronic structure and magnetic properties of high-spin octahedral Co(II) complexes: $Co(II)(acac)_2(H_2O)_2$. *J. Chem. Phys.* **1999**, *111*, 10148. (b) Papánková, B.; Boča, R.; Dlháň, L.; Nemec, I.; Titiš, J.; Svoboda, I.; Fuess, H. Magneto-structural relationships for a mononuclear Co(II) complex with large zero-field splitting. *Inorg. Chim. Acta* **2010**, *363*, 147. (c) Jankovics, H.; Daskalakis, M.; Raptopoulou, C. P.; Terzis, A.; Tangoulis, V.; Giapintzakis, J.; Kiss, N.; Salifoglou, A. Synthesis and Structural and Spectroscopic Characterization of a Complex between Co(II) and Imino-bis(methyl-phosphonic acid): Gaining Insight into Biologically Relevant Metal–Ion Phosphonate Interactions or Looking at a New Co(II)–Organophosphonate Material. *Inorg. Chem.* **2002**, *41*, 3366. (d) Váhovská, L.; Potočňák, I.; Vitushkina, S.; Dušek, M.; Titiš, J.; Boča, R. Low-dimensional compounds containing cyanido groups. XXVI. Crystal structure, spectroscopic and magnetic properties of Co(II) complexes with non-linear pseudohalide ligands. *Polyhedron* **2014**, *81*, 396.
(19) Titiš, J.; Boča, R. Magnetostructural *D* Correlations in Hexacoordinated Cobalt(II) Complexes. *Inorg. Chem.* **2011**, *50*, 11838.
(20) Idešicová, M.; Boča, R. Magnetism, IR and Raman spectra of a tetracoordinate and hexacoordinate Co(II) complexes derived from aminopyrimidine. *Inorg. Chim. Acta* **2013**, *408*, 162.
(21) Boča, R. *Program MIF;* University of SS Cyril and Methodius: Trnava, Slovakia, 2015.
(22) Carlin, R. L. *Magnetochemistry*; Springer: Berlin, Germany, 1986; p 49.
(23) Herchel, R.; Váhovská, L.; Potočňák, I.; Trávníček, Z. Slow magnetic relaxation in octahedral cobalt(II) field-induced single-ion magnet with positive axial and large rhombic anisotropy. *Inorg. Chem.* **2014**, *53*, 5896.
(24) Smolko, L.; Černák, J.; Dušek, M.; Miklovič, J.; Titiš, J.; Boča, R. Three tetracoordinate Co(II) complexes $[Co(biq)X_2]$ (X = Cl, Br, I) with easy-plane magnetic anisotropy as field-induced single-molecule magnets. *Dalton Trans.* **2015**, *44*, 17565.
(25) Packová, A.; Miklovič, J.; Boča, R. Manifold relaxation processes in a mononuclear Co(II) single-molecule magnet. *Polyhedron* **2015**, *102*, 88.
(26) Boča, R.; Miklovič, J.; Titiš, J. Simple Mononuclear Cobalt(II) Complex: A Single-Molecule Magnet Showing Two Slow Relaxation Processes. *Inorg. Chem.* **2014**, *53*, 2367.
(27) (a) Rajnák, C.; Titiš, J.; Fuhr, O.; Ruben, M.; Boča, R. Single-Molecule Magnetism in a Pentacoordinate Cobalt(II) Complex Supported by an Antenna Ligand. *Inorg. Chem.* **2014**, *53*, 8200. (b) Rajnák, C.; Titiš, J.; Miklovič, J.; Kostakis, G. E.; Fuhr, O.; Ruben, M.; Boča, R. Five mononuclear pentacoordinate Co(II) complexes as field-induced single-molecule magnets. *Polyhedron* **2017**, *126*, 174.
(28) (a) Miklovič, J.; Valigura, D.; Boča, R.; Titiš, J. A mononuclear Ni(II) complex: a field induced single-molecule magnet showing two slow relaxation processes. *Dalton Trans.* **2015**, *44*, 12484. (b) Boča, R.; Rajnák, C.; Titiš, J.; Valigura, D. Field Supported Slow Magnetic Relaxation in a Mononuclear Cu(II) Complex. *Inorg. Chem.* **2017**, *56*, 1478.
(29) Benniston, A. C.; Melnic, S.; Turta, C.; Arauzo, A. B.; Bartolomé, J.; Bartolomé, E.; Harrington, R. W.; Probert, M. R. Preparation and properties of a calcium(II)-based molecular chain decorated with manganese(II) butterfly-like complexes. *Dalton Trans.* **2014**, *43*, 13349.
(30) Dolai, M.; Ali, M.; Titiš, J.; Boča, R. Cu(II)–Dy(III) and Co(III)–Dy(III) based single-molecule magnets with multiple slow magnetic relaxation processes in the Cu(II)–Dy(III) complex. *Dalton Trans.* **2015**, *44*, 13242.

DOI: 10.1021/acs.inorgchem.7b00605
Inorg. Chem. 2017, 56, 6999–7009